REPORT

PHYSICS

Electron-phonon instability in graphene revealed by global and local noise probes

Trond I. Andersen[1]*, Bo L. Dwyer[1]*, Javier D. Sanchez-Yamagishi[2]*, Joaquin F. Rodriguez-Nieva[1], Kartiek Agarwal[3], Kenji Watanabe[4], Takashi Taniguchi[4], Eugene A. Demler[1], Philip Kim[1,5], Hongkun Park[1,6], Mikhail D. Lukin[1]†

Understanding and controlling nonequilibrium electronic phenomena is an outstanding challenge in science and engineering. By electrically driving ultraclean graphene devices out of equilibrium, we observe an instability that is manifested as substantially enhanced current fluctuations and suppressed conductivity at microwave frequencies. Spatial mapping of the nonequilibrium current fluctuations using nanoscale magnetic field sensors reveals that the fluctuations grow exponentially along the direction of carrier flow. Our observations, including the dependence on density and temperature, are consistently explained by the emergence of an electron-phonon Cerenkov instability at supersonic drift velocities. These results offer the opportunity for tunable terahertz generation and active phononic devices based on two-dimensional materials.

Nonequilibrium phenomena in driven electronic and optical systems display rich dynamics that can be harnessed for applications such as Gunn diodes and lasers. Two-dimensional (2D) materials (*1*) constitute a new platform for exploring such nonequilibrium phenomena. In particular, modern ultraclean graphene devices exhibit high mobilities (*2*) and can be driven to high electronic drift velocities where instabilities have been predicted to occur. Examples include hydrodynamic instabilities (*3*) in electronic fluids (*4*, *5*), as well as Dyakonov-Shur instabilities, where plasmons are amplified by driven electrons (*6*, *7*). In addition to the potential use for high-frequency signal generation, understanding nonequilibrium dynamics is vital for many technological applications of graphene, including high-frequency transistors (*8*), ultrafast incandescent light sources (*9*), and flexible transparent interconnects (*10*). In practice, such electronic instabilities are difficult to realize owing to increased phonon scattering at high drift velocities. Although phonon scattering is typically an irreversible loss channel, long-lived phonons can themselves act as a source of instabilities. Specifically, when the electronic drift velocity (v_D) exceeds the sound velocity (v_s), stimulated phonon emission can dominate over absorption (Fig. 1B), resulting in exponential growth of the phonon population known as phonon Cerenkov amplification (*11*, *12*). This phenomenon has long been theoretically explored as a method to produce high-frequency acoustic waves (*13*, *14*), with experimental evidence found in bulk systems and semiconductor superlattices via acoustic and optical measurements (*15*–*18*).

Our experiments make use of electrically gated graphene devices encapsulated in hexagonal boron nitride (hBN) (Fig. 1A) and are conducted at cryogenic temperatures (T = 10 to 80 K). Figure 1C presents the low-bias transport properties of the ultraclean graphene system, with a mobility of 20 to 40 $m^2/V{\cdot}s$ at a carrier density, n, of 2×10^{12} cm^{-2}, corresponding to nearly ballistic transport (*19*). Due to the high mobility, carriers can be accelerated by an electric field to high drift velocities ($v_D \gg v_s = 21$ km/s), where a nonlinear current response is observed (Fig. 1D, blue). By contrast, a disordered device shows linear ohmic behavior (Fig. 1D, black).

We first study the nonequilibrium behavior by measuring the global noise in the source-drain current with a spectrum analyzer (noise power spectral density, PSD, averaged over 0.1 to 0.3 GHz), while varying the applied bias power, P. The noise observed in disordered devices (Fig. 1E, black) is in good agreement with increased thermal noise due to Joule heating and shows a characteristic $P^{1/3}$-dependence (*19*, *20*). Different behavior is observed in clean (hBN-encapsulated) devices, where the noise grows superlinearly with drive power and reaches values that are inconsistent with thermal noise. In particular, at higher biases, the noise increases to values equivalent to the thermal noise expected for a sample at 10,000 K (*19*). This behavior, observed consistently in 12 devices (*19*), stands in stark contrast to that of more disordered (not hBN-encapsulated) devices studied here and elsewhere (*20*, *21*), indicating a new noise source in driven graphene devices with low disorder.

To gain insights into the origin of this anomalous noise, we perform spatially resolved noise measurements by fabricating graphene devices on diamond substrates that contain shallow nitrogen-vacancy (NV) color-center impurities (40 to 60 nm depth) (*19*, *22*). These atomlike spin qubits can be individually measured using confocal microscopy and can probe nanoscale current noise by measuring the resulting magnetic fields (*23*–*25*). The locally probed noise under a driven clean graphene device exhibits similar superlinear behavior as global measurements (Fig. 1F).

We probe the spatial dependence of the anomalous noise by optically addressing single NV centers along the device (Fig. 2A) and measuring their spin relaxation rate (Fig. 2B), which is determined by the local noise at 2.87 GHz (*23*). Far from the midpoint of the device, the noise exhibits a clear asymmetry with current direction (Fig. 2C), with nearly an order of magnitude difference when the current is reversed. This is surprising given that the global noise and transport properties are independent of current direction (*19*). Using the device gate, we invert the sign of the charge carriers and find that the asymmetric pattern also inverts, indicating that the local noise signal depends on the flow direction of momentum, not charge. Figure 2D shows the local noise profile along the source-drain direction when $v_D = 5.8v_s$. We observe that the noise is small at the carrier entry point but then grows exponentially as the carriers flow down the 17-μm-long device. The noise profile inverts when the current direction is reversed and flips back when the carrier sign is also switched (Fig. 2E).

To explore the underlying dynamics, we measure the spectrum of the global current noise. When driven, the disordered graphene samples show $1/f$ noise and white thermal noise (Fig. 3A, black curve), consistent with previous studies (*20*, *26*). Clean devices, on the other hand, exhibit a peaked spectrum with a roll-off at ~1.5 GHz. The ac differential conductivity is suppressed at similar frequencies (Fig. 3B). These gigahertz features are in stark contrast to the equilibrium graphene Drude spectrum, which is featureless up to terahertz frequencies (*27*, *28*), thus indicating time scales much longer than the typical electronic lifetime. The frequencies of these nonequilibrium features are independent of drive voltage, doping, and temperature (*19*), but they are upshifted in a shorter device (Fig. 3, C and D).

The observed spectrum, spatial dependence, and scale of the anomalous noise are inconsistent

[1]Department of Physics, Harvard University, Cambridge, MA 02138, USA. [2]Department of Physics and Astronomy, University of California, Irvine, Irvine, CA 92697, USA. [3]Department of Physics, McGill University, Montréal, Québec H3A 2T8, Canada. [4]National Institute for Materials Science, Namiki 1-1, Tsukuba, Ibaraki 305-0044, Japan. [5]John A. Paulson School of Engineering and Applied Sciences, Harvard University, Cambridge, MA 02138, USA. [6]Department of Chemistry and Chemical Biology, Harvard University, Cambridge, MA 02138, USA.
*These authors contributed equally to this work.
†Corresponding author. Email: lukin@physics.harvard.edu

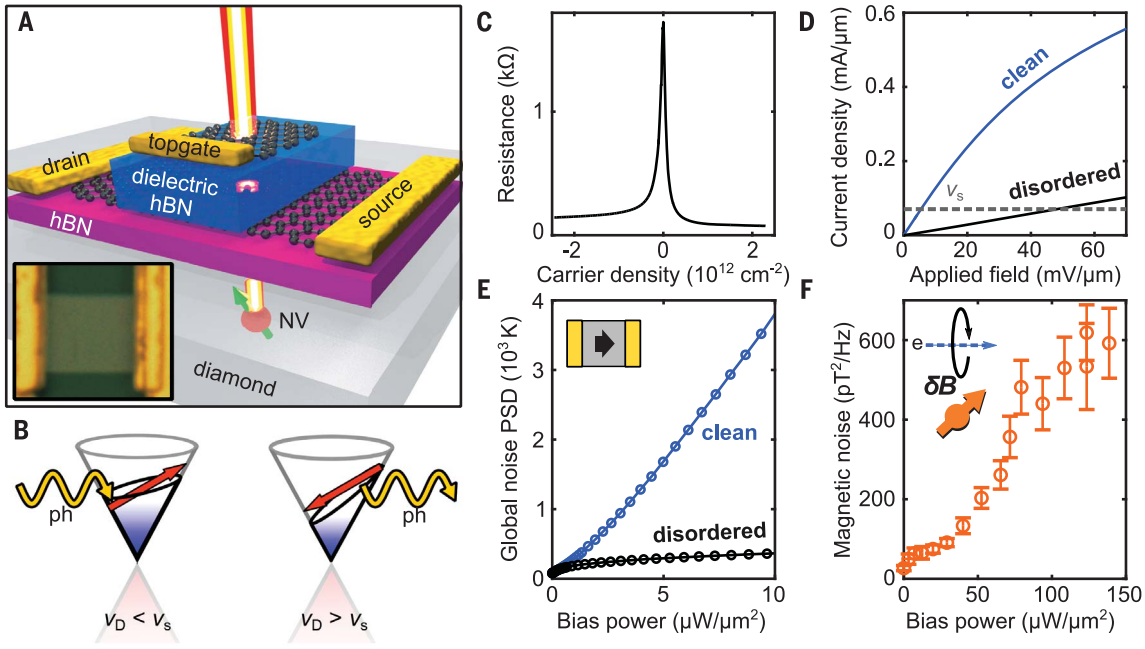

Fig. 1. Nonequilibrium dynamics in graphene, probed both globally and locally. (**A**) Device schematic: hBN-encapsulated graphene device on diamond substrate containing NV centers for nanomagnetometry. (Inset) Optical image of clean hBN-encapsulated device A1 (6 μm by 5.4 μm). (**B**) Condition for Cerenkov emission of phonons: when $v_D > v_s$, stimulated phonon (ph) emission dominates over absorption (right). (**C**) Two-probe resistance versus carrier density of device A1 (T = 10 K). (**D**) Current density as a function of applied electric field (T = 80 K) in clean device A1 (blue) and disordered device B1 (7 μm by 18 μm, black). The gray dashed line indicates where $v_D = v_s$ for the longitudinal acoustic mode. (**E**) Global electronic noise PSD (averaged over 100 to 300 MHz) as a function of bias power in devices A1 (blue) and B1 (black). Blue curve satisfies $v_D > v_s$ for $P > 0.12$ μW/μm^2. (**F**) Local magnetic noise (measured by NV nanomagnetometry) versus applied bias power in clean device C1 on diamond substrate. Error bars represent 95% confidence intervals.

with conventional noise sources (such as $1/f$ or white thermal/shot noise) (*29*). Our observations, especially the slow time scales and their independence on electronic parameters, are incompatible with many purely electronic mechanisms for ac signal generation (*3*, *6*, *19*, *30*) and suggest that other, longer-lived excitations play a role. In particular, the time scales match well with the time it takes for acoustic phonons to traverse the device. Furthermore, the anomalous effects occur only when the electronic drift velocity is higher than the speed of sound, but emerge at energies that are too low to excite optical phonons and plasmons ($2\hbar k_F v_D$, $k_B T <$ 20 meV, where $\hbar$ is the reduced Planck constant, k_F is the Fermi wavevector, and k_B is the Boltzmann constant) (*19*).

All of our observations are consistently explained as an electron-phonon Cerenkov instability. The key insight is that when the electronic drift velocity exceeds the speed of sound, a cone of forward-moving acoustic phonon modes experiences a faster rate of stimulated emission ($\gamma_{\mathbf{q}}^{\mathrm{em}}$) than absorption ($\gamma_{\mathbf{q}}^{\mathrm{abs}}$) (*11*–*14*). For the emitted phonons to amplify, $\gamma_{\mathbf{q}}^{\mathrm{em}}$ must exceed the loss rate due to absorption and other decay sources. Pristine graphene exhibits long acoustic phonon lifetimes ($\tau_{\mathbf{q}}$) (*31*), thus an emitted phonon can stimulate the emission of more phonons, leading to exponential growth (Fig. 3G). This process is seeded by a wide spectrum of spontaneously emitted and thermal phonons and is therefore expected to have limited coherence. Stochastic electronic scattering with the growing phonon population is expected to reduce the conductivity and increase noise.

To model these effects, we analyze the coupled electron-phonon dynamics by including the influence of the phonons on the electronic scattering rate, Γ_e (*19*)

$$\partial_t \mathbf{j}(\mathbf{r},t) = D\mathbf{E}(\mathbf{r},t) - \Gamma_e(\{n_{\mathbf{q}}\})\mathbf{j}(\mathbf{r},t) \quad (1)$$

$$\partial_t n_{\mathbf{q}} = -\frac{(n_{\mathbf{q}} - n_{\mathbf{q},0})}{\tau_{\mathbf{q}}} + \gamma_{\mathbf{q}}^{\mathrm{em}}(\mathbf{j})(n_{\mathbf{q}}+1) - \gamma_{\mathbf{q}}^{\mathrm{abs}}(\mathbf{j})n_{\mathbf{q}} - v_s\hat{\mathbf{q}}\cdot\nabla n_{\mathbf{q}} \quad (2)$$

Here, $D = 2e^2 v_F k_F/h$ is the Drude weight of graphene, $\mathbf{E}(\mathbf{r},t)$ is the electric field, $n_{\mathbf{q}}$ is the phonon occupation at wavevector $\mathbf{q}$, $n_{\mathbf{q},0}$ is the equilibrium phonon occupation when the current density, $\mathbf{j}$, is zero, and $\tau_{\mathbf{q}}^{-1}$ is assumed to be dominated by anharmonic interactions. Although we describe the phonon population using second quantization, the results can also be obtained through a semiclassical treatment. Using known constants for the electron-phonon coupling and anharmonic decay, we find that phonon amplification ($\Gamma_{\mathbf{q}}^{\mathrm{amp}} = \gamma_{\mathbf{q}}^{\mathrm{em}} - \gamma_{\mathbf{q}}^{\mathrm{abs}} - \tau_{\mathbf{q}}^{-1} > 0$) can be easily achieved for a wide range of parameters (*19*). For instance, the parameters used in Fig. 2D ($v_D = 5.8 v_s$) give a maximum $\gamma_{\mathbf{q}}^{\mathrm{em}} - \gamma_{\mathbf{q}}^{\mathrm{abs}} = 11$ GHz at $q \sim 2\pi/(25\,\mathrm{nm})$, where $\tau_{\mathbf{q}}^{-1} = 0.02$ GHz. The amplification of stochastically emitted phonons is expected to cause large fluctuations in the local electronic scattering rate, thus generating current noise. Due to the Poissonian nature of phonon emission, the fluctuations are expected to scale with the mean emission rate, which is proportional to $n_{\mathbf{q}}$. We thus plot the spatial profile of the excess phonon population ($\sim e^{\Gamma^{\mathrm{amp}} x/v_s} - 1$) associated with $\Gamma^{\mathrm{amp}} = 11$ GHz (dashed black curve) along with the noise profile in Fig. 2D, and find good agreement with our experimental results. Integrating over more modes gives a similar profile, indicating the dominance of the most-amplified modes (*19*). This amplification behavior is also consistent with our global measurements, where the anomalous noise increases with device length (*19*).

The model also predicts that the electron-phonon Cerenkov instability gives rise to a conductivity spectrum of the form

$$\sigma(\omega) = \frac{\sigma^{\mathrm{Drude}}(0)}{1 - \frac{iK}{\omega t_T}(1 - e^{-i\omega t_T})} \quad (3)$$

where $\sigma^{\mathrm{Drude}}(0) = D/\Gamma_e$ is the usual dc Drude conductivity and K is an increasing function of $\Gamma_{\mathbf{q}}^{\mathrm{amp}}$ (*19*). Importantly, $\sigma(\omega)$ depends on the sample traversal time for phonons, $t_T = L/v_s$, where L

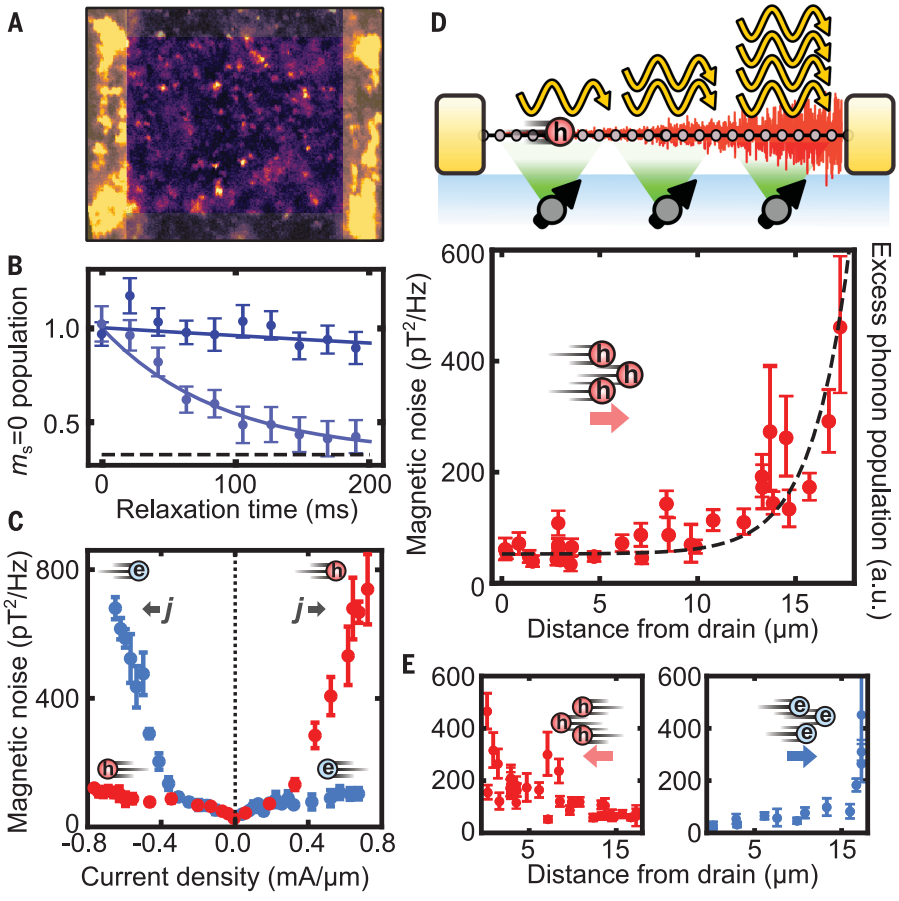

Fig. 2. Spatially resolved local noise measurements with NV magnetometry. (**A**) Fluorescence image of NV centers underneath device C2, with false-colored contacts and borders added. (**B**) NV spin relaxation from polarized to thermal state (dashed line), when current densities j = 0 mA/μm (dark blue) and j = −0.19 mA/μm (light blue) are passed through the device. Solid lines are fits. m_s, spin quantum number. (**C**) Local magnetic noise near drain contact as a function of graphene current density (device C1) in electron (e)– and hole (h)–doped regime (blue and red, respectively). (**D**) Spatial map of the local magnetic noise (device C2) at j = 0.18 mA/μm and $n = 0.92 \times 10^{12}$ cm^{-2}. The spatial profile is consistent with the exponential growth of phonons due to Cerenkov amplification (cartoon, top). Dashed black curve shows the theoretically predicted excess phonon population (offset to account for background noise). a.u., arbitrary units. (**E**) The growth direction is reversed by changing the current direction (left) or the charge carrier sign (right). Error bars represent 95% confidence intervals.

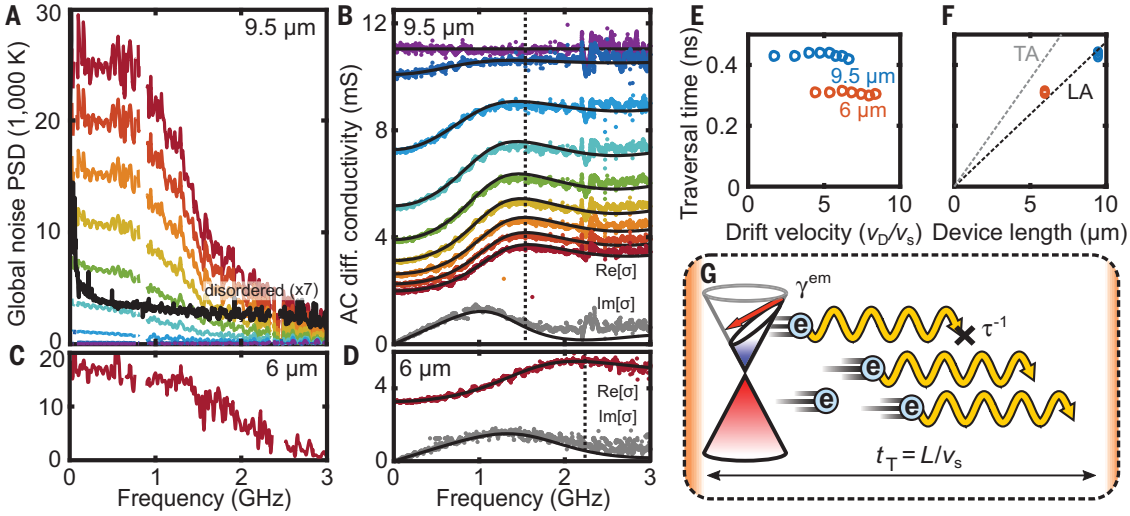

Fig. 3. Slow dynamics in global electronic measurements. (**A**) Global noise spectra at $n = 2 \times 10^{12}$ cm^{-2}. Colored curves: clean device A2 (9.5 μm by 11 μm) at bias ranging from 0 to 0.8 V (bottom to top). Black curve: disordered device B1 at maximum power applied to device A2 (scaled 7×). (**B**) Ac differential conductivity spectra (excitation: −20 dBm) (*19*) with biases 0 to 0.8 V [top to bottom, colors same as in (A)]. The real (Re) component is suppressed at low frequencies. Gray curve: imaginary (Im) component at 0.8 V. Black curves are fits. (**C** and **D**) Features in noise and conductivity spectra shift to higher frequencies in a shorter (6-μm) device (device A1) under similar electric field as maximum in (A) and (B). (**E** and **F**) Extracted traversal time from (B) and (D) as a function of drift velocity and device length. Dashed curves correspond to speed of sound in graphene [light gray, transverse acoustic (TA); dark gray, longitudinal acoustic (LA)]. (**G**) Cartoon of important rates in the driven electron-phonon system. During Cerenkov amplification, the correlation time observed in electronic measurements is limited by the phonon traversal time, $t_T = L/v_s$.

is the device length. When Cerenkov amplification occurs, the correlation time probed in conductivity measurements is no longer limited by the individual electron and phonon lifetimes but by the traversal time, because the memory of an emission event is amplified until the phonons reach the edge (reflected, backward-moving modes are no longer amplified). To account for the variation in t_T with phonon emission angle, we sum over a cone in phonon phase space in our fits (*19*). Our model gives excellent agreement with the observed conductivity spectra (Fig. 3, B and D, black curves) and even predicts the slight oscillatory behavior due to the sharp transit time cutoff. The extracted traversal time is

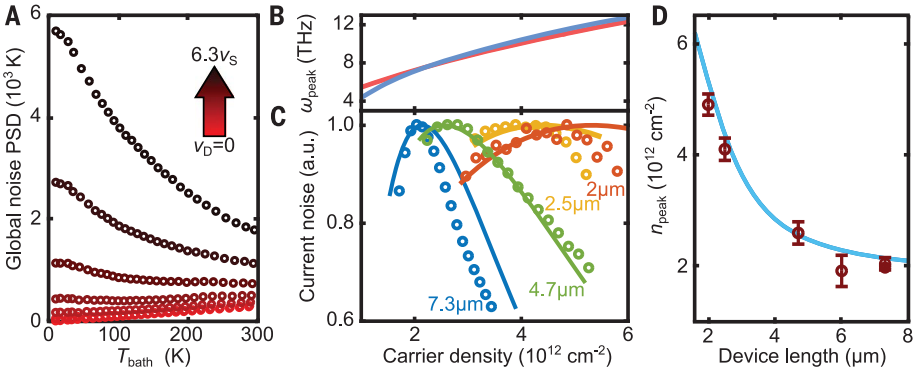

Fig. 4. Dependence on bath temperature and charge density. (**A**) Global noise PSD as a function of bath temperature at constant drift velocities and $n = 2 \times 10^{12}$ cm^{-2}. (**B**) Calculated peak phonon emission frequency, which can be tuned via the graphene carrier density (blue: $T_e = 0$ K; red: $T_e = 320$ K). (**C**) Normalized global current noise as a function of carrier density for different device lengths ($j = 0.6$ mA/μm). Solid curves show predicted total phonon emission. (**D**) The charge density at which the noise peaks (n_{peak}) for a wider variety of samples than in (C), with fit (blue). Error bars represent sampling spacing of carrier densities.

independent of drift velocity (Fig. 3E), and the corresponding speed matches that of the longitudinal acoustic mode in graphene (Fig. 3F) (*32*).

The extension of the correlation time is expected to also cause noise in the same low-frequency range, consistent with our observations (Fig. 3, A and C). Whereas the stochastic emission of a phonon normally causes a small drop in current that only lasts for $1/\Gamma_e \sim$ picoseconds, Cerenkov amplification both prolongs and magnifies the effect. The emitted phonon stimulates cascading emission of subsequent phonons, causing the current to continue decreasing until the phonon packet reaches the device edge. This should give strong current correlations $\langle \delta j(t) \delta j(t+\tau) \rangle$ for long τ (up to $t_T \sim 100$ ps) and thus noise at low frequencies $\lesssim 1/t_T$.

Cerenkov amplification is sensitive to the phonon lifetime, and the effect is therefore expected to intensify at lower temperatures because of slower anharmonic decay (*33*). We observe a strong increase in noise as the temperature is reduced from 300 to 10 K (Fig. 4A), in clear contrast to the decreasing thermal noise observed at low drives ($v_D \lesssim v_s$). This suggests that the amplification process is limited by scattering with thermally occupied modes at energies similar to that of the amplified mode (7 THz ~ 50 K at $n = 2 \times 10^{12}$ cm^{-2}).

Another important aspect of Cerenkov amplification in graphene is that the peak emission frequency is tunable via the carrier density, n (Fig. 4B). This peak occurs just below the upper limit $\omega \sim 2v_s k_F$, corresponding to transitions across the entire Fermi surface. The frequency tunability manifests as a nonmonotonic dependence of the global current noise on n (Fig. 4C) (*19*). Initially, the noise increases with n, because the larger Fermi surface permits emission of more (and higher-energy) modes. In other words, increasing n broadens $\Gamma_{\mathbf{q}}^{amp}$. However, its maximum value decreases at constant current because $v_D = j/ne$, eventually causing a downturn in noise.

The crossover density, n_{peak}, is determined by the relative importance of the width and maximum of $\Gamma_{\mathbf{q}}^{amp}$, which depends on the device length. Analogously to an active filter, the amplification process narrows the excess phonon distribution $n_{\mathbf{q}}(x) \sim e^{\Gamma_{\mathbf{q}}^{amp} x/v_s}$ as it traverses the device. In longer devices, the noise therefore depends more on the maximum of $\Gamma_{\mathbf{q}}^{amp}$ than its width, causing a smaller n_{peak}. We observe such a length dependence, shown in Fig. 4, C and D in terms of current noise to facilitate comparison with the model. Plotting the predicted total phonon emission along with the data, we find that our model reproduces both the peak shift and narrowing well (*19*).

These considerations show that our observations are well explained as an electron-phonon Cerenkov instability in a 2D material. This driven electron-phonon system shows rich nonequilibrium dynamics that merit further exploration, potentially by developing new techniques to directly characterize the phonon spectrum. Prior theoretical work predicts that the amplified phonons in graphene have frequencies as high as 10 THz (*14*), substantially higher than those observed in other materials (*15*, *16*, *18*). Moreover, this system can offer purely electrical generation and amplification of phonons in a single micrometer-scale device, with wide frequency tunability. Future work could explore coupling to a mechanical cavity to develop a phononic laser, as well as outcoupling of the amplified sound waves to far-field terahertz radiation. Our results represent a promising step toward a new generation of active phononic and photonic devices based on 2D materials.

REFERENCES AND NOTES

1. K. S. Novoselov, A. Mishchenko, A. Carvalho, A. H. Castro Neto, *Science* **353**, aac9439 (2016).
2. L. Wang *et al.*, *Science* **342**, 614–617 (2013).
3. M. Mendoza, H. J. Herrmann, S. Succi, *Phys. Rev. Lett.* **106**, 156601 (2011).
4. R. Krishna Kumar *et al.*, *Nat. Phys.* **13**, 1182–1185 (2017).
5. J. Crossno *et al.*, *Science* **351**, 1058–1061 (2016).
6. M. Dyakonov, M. Shur, *Phys. Rev. Lett.* **71**, 2465–2468 (1993).
7. A. Tomadin, M. Polini, *Phys. Rev. B* **88**, 205426 (2013).
8. Y.-M. Lin *et al.*, *Science* **327**, 662 (2010).
9. Y. D. Kim *et al.*, *Nano Lett.* **18**, 934–940 (2018).
10. R.-H. Kim *et al.*, *Nano Lett.* **11**, 3881–3886 (2011).
11. A. Pippard, *Philos. Mag.* **8**, 161–165 (1963).
12. H. N. Spector, *Phys. Rev.* **127**, 1084–1090 (1962).
13. S. M. Komirenko, K. W. Kim, A. A. Demidenko, V. A. Kochelap, M. A. Stroscio, *Phys. Rev. B* **62**, 7459–7469 (2000).
14. C. X. Zhao, W. Xu, F. M. Peeters, *Appl. Phys. Lett.* **102**, 222101 (2013).
15. A. R. Hutson, J. H. McFee, D. L. White, *Phys. Rev. Lett.* **7**, 237–239 (1961).
16. M. Pomerantz, *Phys. Rev. Lett.* **13**, 308–310 (1964).
17. M. Eizenberg, B. Fisher, *J. Appl. Phys.* **49**, 5260–5269 (1978).
18. K. Shinokita *et al.*, *Phys. Rev. Lett.* **116**, 075504 (2016).
19. See supplementary materials.
20. A. Betz *et al.*, *Nat. Phys.* **9**, 109–112 (2013).
21. W. Yang *et al.*, *Nat. Nanotechnol.* **13**, 47–52 (2018).
22. J. R. Maze *et al.*, *Nature* **455**, 644–647 (2008).
23. S. Kolkowitz *et al.*, *Science* **347**, 1129–1132 (2015).
24. K. Agarwal *et al.*, *Phys. Rev. B* **95**, 155107 (2017).
25. F. Casola, T. van der Sar, A. Yacoby, *Nat. Rev. Mater.* **3**, 17088 (2018).
26. A. A. Balandin, *Nat. Nanotechnol.* **8**, 549–555 (2013).
27. J. Horng *et al.*, *Phys. Rev. B* **83**, 165113 (2011).
28. S. Awan *et al.*, *2D Mater.* **3**, 015010 (2016).
29. H. L. Hartnagel, R. Katilius, A. Matulionis, *Microwave Noise in Semiconductor Devices* (Wiley, 2001).
30. S. A. Mikhailov, *Phys. Rev. B* **87**, 115405 (2013).
31. D. L. Nika, E. P. Pokatilov, A. S. Askerov, A. A. Balandin, *Phys. Rev. B* **79**, 155413 (2009).
32. K. Kaasbjerg, K. S. Thygesen, K. W. Jacobsen, *Phys. Rev. B* **85**, 165440 (2012).
33. P. Klemens, D. Pedraza, *Carbon* **32**, 735–741 (1994).

ACKNOWLEDGMENTS

We thank J. Waissman, A. Talanov, B. Halperin, L. Levitov, D. Ham, K. de Greve, A. Safira, and K. C. Fong for helpful discussions. **Funding:** T.I.A., B.L.D., J.D.S.-Y., and M.D.L. acknowledge financial support from the Center for Ultracold Atoms, the National Science Foundation (NSF), the Department of Defense Vannevar Bush Faculty Fellowship, and the Gordon and Betty Moore Foundation. All fabrication was performed at the Center for Nanoscale Systems (CNS), a member of the National Nanotechnology Coordinated Infrastructure Network (NNCI), which is supported by the National Science Foundation under NSF award 1541959. CNS is part of Harvard University. K.A. acknowledges support from the UK Foundation. K.W. and T.T. acknowledge support from the Elemental Strategy Initiative conducted by the MEXT, Japan and the CREST (JPMJCR15F3), JST. P.K. acknowledges support from ARO (W911NF-17-1-0574). **Author contributions:** T.I.A., B.L.D., J.D.S.-Y., and K.A. conceived of the project. T.I.A., B.L.D., and J.D.S.-Y. designed and performed the experiments, fabricated the devices, analyzed the data, and wrote the manuscript. T.I.A., K.A., and J.F.R.-N. developed the theoretical model. T.T. and K.W. grew the hBN crystals. E.A.D., P.K., H.P., and M.D.L. supervised the project. **Competing interests:** The authors declare no competing interests. **Data and materials availability:** All data needed to evaluate the conclusions in the paper are present in the paper and the supplementary materials.

SUPPLEMENTARY MATERIALS

www.sciencemag.org/content/364/6436/154/suppl/DC1
Materials and Methods
Supplementary Text
Figs. S1 to S26
Table S1
References (*34*–*60*)

28 November 2018; accepted 14 March 2019
10.1126/science.aaw2104

Electron-phonon instability in graphene revealed by global and local noise probes

Trond I. Andersen, Bo L. Dwyer, Javier D. Sanchez-Yamagishi, Joaquin F. Rodriguez-Nieva, Kartiek Agarwal, Kenji Watanabe, Takashi Taniguchi, Eugene A. Demler, Philip Kim, Hongkun Park and Mikhail D. Lukin

Science **364** (6436), 154-157.
DOI: 10.1126/science.aaw2104

Graphene: Driven to emission

Studying the electronic properties of graphene under extreme nonequilibrium conditions has provided a productive testbed to probe and monitor exotic transport phenomena. Andersen *et al.* report measurements of electron transport in ultraclean graphene devices where the electron drift velocity is extremely high. They found that direct current at high drift velocities generates a large increase in the noise at gigahertz frequencies and that the noise grows exponentially in the direction of the current. The authors attribute the emission mechanism to amplification of acoustic phonons through the Cerenkov effect.

Science, this issue p. 154